

Iterative real-time path integral approach to nonequilibrium quantum transport

S. Weiss, J. Eckel, M. Thorwart and R. Egger

Institut für Theoretische Physik, Heinrich-Heine-Universität Düsseldorf, 40225 Düsseldorf, Germany

(Dated: May 16, 2008)

We have developed a numerical approach to compute real-time path integral expressions for quantum transport problems out of equilibrium. The scheme is based on a deterministic iterative summation of the path integral (ISPI) for the generating function of the nonequilibrium current. Self-energies due to the leads, being non-local in time, are fully taken into account within a finite memory time, thereby including non-Markovian effects, and numerical results are extrapolated both to vanishing (Trotter) time discretization and to infinite memory time. This extrapolation scheme converges except at very low temperatures, and the results are then numerically exact. The method is applied to nonequilibrium transport through an Anderson dot.

PACS numbers: 73.23.-b, 73.23.Hk, 72.10.-d, 02.70.-c

I. INTRODUCTION

Quantum transport has attracted theoretical and experimental research since it offers the possibility to investigate quantum many-body properties at as well as out of thermodynamic equilibrium [1]. The ongoing improvement in miniaturization down to the nanometer scale allows to study electron transport in ultra-small devices, e.g., in single molecules or artificially designed quantum dots [2, 3, 4, 5, 6, 7]. There is a broad variety of interesting physical effects, due to interactions or the nonequilibrium conditions arising when a bias voltage is applied to the source and drain electrodes [8, 9, 10]. These range from Coulomb blockade via coherent (e.g., resonant tunneling) transport to the Kondo effect, to name but a few. While on the experimental side, progress stems from an increased control of fabrication processes, many theoretical works deal with refined approximation schemes applicable in different parameter regimes. However, *exact* theoretical results — either analytical or numerical — for nonequilibrium quantum transport systems are rare, mainly because of the lack of adequate methods allowing to tackle such questions. There clearly is a considerable need for numerically exact methods to describe nonequilibrium quantum transport, both to check analytical (and usually approximate) approaches and to connect theory to experiment. Here, we mean by nonequilibrium transport specifically those phenomena which go beyond the standard approach of linear response to the applied bias voltage.

In this work, we propose a novel numerical scheme denoted as *iterative summation of real-time path integrals* (ISPI), in order to address quantum transport problems out of equilibrium. Many-body systems driven out of equilibrium are known [11, 12, 13] to acquire a steady state that may be quite different in character from their ground-state properties. Details of the steady state may depend on the nature of the correlations, as well as on the way in which the system is driven out of equilibrium. While there are a variety of nonperturbative techniques in place to study equilibrium systems, many of these methods cannot be extended to nonequilibrium systems

in a straightforward way.

Different approximations have been pursued previously in order to tackle nonequilibrium situations. For instance, transport through an Anderson dot in the Kondo regime has been described theoretically along several different lines, e.g., for the asymptotic low-energy regime by Fermi liquid theory [14], via interpolative schemes [15], using integrability concepts [16], or by the perturbative renormalization group [12, 17]. Transport features of the Anderson model have also been discussed by perturbation theory in the interaction strength [18, 19]. Sophisticated nonperturbative methods have been developed in order to extract exact results out of equilibrium for special models, where integrability is available. For instance, the interacting resonant level model presently enjoys much interest [20, 21, 22, 23, 24, 25, 26]. Universal aspects of nonequilibrium currents in a quantum dot have been discussed in Ref. [21]. In various perturbative regimes, this model has been addressed by field theory methods [23, 24, 25, 26]. However, the underlying theoretical concepts are still under much debate, and partially conflicting results were reported in the literature, cf. Refs. [23, 24, 25].

The above discussion shows that precise numerical simulation tools are in great demand in this field. Let us briefly review the existing numerical methods available for nonequilibrium transport. Much effort has been directed to the application of renormalization group (RG) techniques to this problem. For instance, a perturbative real-time RG analysis of nonequilibrium transport has been performed [27], and steps towards the appropriate generalization of the density matrix renormalization group technique have appeared [28, 29]. In addition, the functional RG approach has been generalized to nonequilibrium recently [30]. It forms a systematic and fast perturbative expansion scheme, yielding reliable results for small interaction strengths, where the infinite hierarchy of equations for the self-energy can be cut after the first few steps. Moreover, a possible extension of Wilson's numerical RG approach to nonequilibrium has been discussed [31, 32]. Another line of attack considered numerically exact real-time quantum Monte Carlo (QMC)

simulations (for the corresponding equilibrium case, see Refs. [33, 34]). Due to the sign problem, however, these calculations become increasingly difficult at low temperatures. Refined multi-level blocking techniques [35, 36] allow to achieve further progress, but numerical simulations remain hard within this approach. (For recent progress, however, see Ref [37].) Let us also mention the flow equation method, which has been applied to study the nonequilibrium Kondo effect [38]. Finally, a very recent development considers non-standard ensembles to describe steady state transport, but involves a numerically troublesome analytic continuation [39].

Our ISPI approach, described in detail below, provides a novel alternative, and in principle numerically exact, method to tackle out-of-equilibrium transport through correlated quantum dots. The method is deterministic and, hence, there is no sign problem. It is based on the evaluation of the full nonequilibrium Keldysh generating function, including suitable source terms to generate the observables of interest. It builds on the fact that the fermionic leads induce self-energies that are non-local in time, but which decay exponentially in the long-time limit at any finite temperature. Thus, a memory time exists such that within this time span, the correlations are exactly taken into account, while for larger times, the correlations can be dropped. This allows to construct an iterative scheme to evaluate the generating function. An appropriate extrapolation procedure allows then to eliminate both the Trotter time discretization error (the Hubbard-Stratonovich (HS) transformation below requires to discretize time), and the finite memory-time error, yielding finally the desired numerically exact value for the observables of interest. The extrapolation procedure is convergent for not too low temperatures, since then memory effects are exponentially small for long times. If the extrapolation converges, we thereby obtain numerically exact results for nonequilibrium quantum transport properties of interacting systems.

The ISPI scheme is implemented here for the example of the well-known single-level Anderson impurity model [40, 41, 42, 43, 44], but appropriately modified, it can be applied to other quantum dot models as well. The nonequilibrium current is calculated from a generating function, represented as a real-time path integral in the Keldysh formalism. After a Hubbard-Stratonovich transformation employing an auxiliary Ising spin field, all fermionic degrees of freedom (of the dot and the leads) can be integrated out exactly, however, at the price of introducing time-nonlocal self-energies for the leads and a path summation over all Ising spin configurations. For this, an iterative summation scheme is constructed, exploiting that the time-nonlocal correlations in the lead self-energy effectively decay exponentially at finite temperature T or bias voltage V , thereby setting the characteristic memory time. For larger times, the correlations are exponentially small and will be neglected. The full time-discretized Keldysh Green's function (GF) of the dot then assumes a band matrix structure, where

the determinant can be calculated iteratively using its Schur form. The scheme is constructed such that within the range set by the memory time, the path integral is evaluated exactly. The remaining systematic errors are the Trotter time discretization and the finite-memory error. Both, however, can be eliminated in a systematic way based on a Hirsch-Fye type extrapolation procedure. Based on the above construction principle, our approach cannot be applied at very low energies ($T, V \rightarrow 0$), where, fortunately, other methods are available. For finite temperatures, the requirement of not too long memory times can be met, and the spin path summation remains tractable.

The present paper is organized as follows. In Sec. II, we introduce the model for the quantum dot coupled to normal leads. We present the computation of the generating function for the nonequilibrium Anderson model in Sec. III in the presence of an external source term, which allows to calculate the current as functional derivative. In Sec. IV we introduce the numerical iterative path-integral summation method, from which we obtain observables of interest. We give a detailed discussion of the convergence properties of our method and describe the extrapolation scheme in Sec. V. For several sets of parameters, we will present results in Sec. VI, followed by a discussion in Sec. VII. Throughout the paper, we set $\hbar = k_B = 1$.

II. MODEL

We consider the Anderson model [40] given by the Hamiltonian

$$\begin{aligned} \mathcal{H} &= H_{dot} + H_{leads} + H_T \\ &= \sum_{\sigma} E_{0\sigma} \hat{n}_{\sigma} + U \hat{n}_{\uparrow} \hat{n}_{\downarrow} + \sum_{kp\sigma} (\epsilon_{kp} - \mu_p) c_{kp\sigma}^{\dagger} c_{kp\sigma} \\ &\quad - \sum_{kp\sigma} \left[t_p c_{kp\sigma}^{\dagger} d_{\sigma} + h.c. \right]. \end{aligned} \quad (1)$$

Here, $E_{0\sigma} = E_0 + \sigma B$ with $\sigma = \uparrow, \downarrow = \pm$ is the energy of a single electron with spin σ on the isolated dot, which can be varied by tuning a back gate voltage or a Zeeman magnetic field term $\propto B$. The latter is assumed not to affect the electron dispersion in the leads. The corresponding dot electron annihilation/creation operator is $d_{\sigma}/d_{\sigma}^{\dagger}$, with $\hat{n}_{\sigma} \equiv d_{\sigma}^{\dagger} d_{\sigma}$ with eigenvalues $n_{\sigma} = 0, 1$, and U denotes the on-dot interaction. For later purpose, it is convenient to use the operator identity $\hat{n}_{\uparrow} \hat{n}_{\downarrow} = \frac{1}{2}(\hat{n}_{\uparrow} + \hat{n}_{\downarrow}) - \frac{1}{2}(\hat{n}_{\uparrow} - \hat{n}_{\downarrow})^2$, thereby introducing the shifted single-particle energies $\epsilon_{0\sigma} \equiv E_{0\sigma} + U/2$, which yields the equivalent dot Hamiltonian

$$H_{dot} = H_{dot,0} + H_U = \sum_{\sigma} \epsilon_{0\sigma} \hat{n}_{\sigma} - \frac{U}{2} (\hat{n}_{\uparrow} - \hat{n}_{\downarrow})^2. \quad (2)$$

In Eq. (1), ϵ_{kp} denotes the energies of the noninteracting electrons (operators $c_{kp\sigma}$) in lead $p = L/R = \pm$, with chemical potential $\mu_p = peV/2$. Dot and leads

are connected by the tunnel couplings t_p . The observable of interest is the (symmetrized) tunneling current $I = (I_L - I_R)/2$,

$$I(t) = -\frac{ie}{2} \sum_{kp\sigma} \left[pt_p \langle c_{kp\sigma}^\dagger d_\sigma \rangle_t - pt_p^* \langle d_\sigma^\dagger c_{kp\sigma} \rangle_t \right], \quad (3)$$

where $I_p(t) = -e\dot{N}_p(t)$ with $N_p(t) = \langle \sum_{k\sigma} c_{kp\sigma}^\dagger c_{kp\sigma} \rangle_t$. The stationary steady-state dc current follows as the asymptotic long-time limit, $I = \lim_{t \rightarrow \infty} I(t)$. We have explicitly confirmed that current conservation, $I_L + I_R = 0$, is numerically fulfilled for the ISPI scheme. In the presence of a finite bias voltage, $V \neq 0$, the Keldysh technique [45, 46, 47] provides a way to study nonequilibrium transport. In this formalism, the time axis is extended to a contour with $\alpha = \pm$ branches, see Fig. 1, along with an effective doubling of fields. The Keldysh GF is $G_{ij}^{\alpha\beta}(t_\alpha, t'_\beta) = -i\langle \mathcal{T}_C[\psi_i(t_\alpha)\psi_j^\dagger(t'_\beta)] \rangle$, where \mathcal{T}_C denotes the contour ordering of times along the Keldysh contour, and $i, j = L, R, 0$ correspond to fields representing lead or dot fermions, respectively. We omit the spin indices here, remembering that each entry still is a diagonal 2×2 matrix in spin space. In general, the four Keldysh components are linearly dependent, such that $G^{++} + G^{--} = G^{+-} + G^{-+}$. However, the commonly used Keldysh rotation [45, 47] seems to offer no advantages here, and is not employed in what follows.

III. GENERATING FUNCTION

Let us then discuss the generating function, which contains all relevant information about the physics of the system. First, we want to integrate out the lead fermion fields, and, in addition, perform a discrete Hubbard-Stratonovich transformation. This allows to integrate out the dot fields as well, and we are then left with a discrete path summation. We start with the fermionic path-integral representation of the generating function,

$$Z[\eta] = \int \mathcal{D} \left[\prod_\sigma \bar{d}_\sigma, d_\sigma, \bar{c}_{kp\sigma}, c_{kp\sigma} \right] e^{iS[\bar{d}_\sigma, d_\sigma, \bar{c}_{kp\sigma}, c_{kp\sigma}]}, \quad (4)$$

with Grassmann fields (\bar{d}, d, \bar{c}, c) (Note that we use the same symbols for fermion operators and Grassmann fields throughout the paper for better readability). We introduce an external source term S_η (defined below in Eq. (6)), which allows to compute the current at measurement time t_m ,

$$I(t_m) = -i \frac{\partial}{\partial \eta} \ln Z[\eta] \Big|_{\eta=0}. \quad (5)$$

We note in passing that it is also possible to evaluate other observables, e.g., the zero-frequency noise, by introducing appropriate source terms and performing the corresponding derivatives. The action is $S = S_{dot} + S_{leads} +$

$S_T + S_\eta$, where

$$\begin{aligned} S_{dot} &= S_{dot,0} + S_U \\ &= \int_C dt \left[\sum_\sigma \bar{d}_\sigma (i\partial_t - \epsilon_{0\sigma}) d_\sigma + \frac{U}{2} (n_\uparrow - n_\downarrow)^2 \right], \\ S_{leads} &= \int_C dt \sum_{kp\sigma} \bar{c}_{kp\sigma} (i\partial_t - \epsilon_{kp} + \mu_p) c_{kp\sigma}, \\ S_T &= \int_C dt \sum_{kp\sigma} t_p \bar{c}_{kp\sigma} d_\sigma + h.c., \\ S_\eta &= \frac{ie\eta}{2} \sum_{kp\sigma} p (t_p \bar{c}_{kp\sigma} d_\sigma - t_p^* \bar{d}_\sigma c_{kp\sigma})(t_m). \end{aligned} \quad (6)$$

The interaction term S_U in Eq. (6) does not allow to directly perform the functional integration. Apart from this, all other terms are quadratic in the Grassmann fields and thus define the ‘noninteracting’ (quadratic) part. Note that the level shift $+U/2$ is here included in the noninteracting sector.

A. Noninteracting part

Before turning to the interacting problem, we briefly discuss the Keldysh GF of the noninteracting problem. Let us first integrate out the lead degrees of freedom. We remain with an effective action for the dot, which is non-local in time due to the presence of the leads. In particular, after Gaussian integration, the generating function reads

$$Z_{ni}[\eta] = \int \mathcal{D} \left[\prod_\sigma \bar{d}_\sigma, d_\sigma \right] e^{i(S_{dot,0} + S_{env})} \quad (7)$$

with

$$\begin{aligned} S_{env} &= \int_C dt \int_C dt' \sum_\sigma \bar{d}_\sigma(t) \left\{ \gamma_L(t, t') + \gamma_R(t, t') \right. \\ &\quad + \frac{ie\eta}{2} [\gamma_L(t, t') - \gamma_R(t, t')] \\ &\quad \left. \times [\delta(t - t_m) - \delta(t' - t_m)] \right\} d_\sigma(t'). \end{aligned} \quad (8)$$

For the source term, the physical measurement time t_m can be taken at one branch of the contour, see Fig. 1. As we fix t_m on the upper (+) branch, the (--) Keldysh element of the source term self-energy vanishes, see the time-discretized version below. The γ_p in Eq. (8) represent the leads, and their Fourier transforms are explicitly given as 2×2 Keldysh matrices,

$$\gamma_p(\omega) = i\Gamma_p \begin{pmatrix} 2f(\omega - \mu_p) - 1 & -2f(\omega - \mu_p) \\ 2 - 2f(\omega - \mu_p) & 2f(\omega - \mu_p) - 1 \end{pmatrix}. \quad (9)$$

Here, we have used the fact that the leads are in thermal equilibrium, $f(\omega) = 1/(e^{\omega/T} + 1)$. Moreover, we take

the standard wide-band limit, with a constant density of states per spin channel around the Fermi energy, $\rho(\epsilon_F)$, yielding the hybridization $\Gamma_p = \pi\rho(\epsilon_F)|t_p|^2$ of the dot level with lead p . For the sake of clarity, we assume from now on symmetric contacts, $\Gamma_L = \Gamma_R \equiv \Gamma/2$. The generalization to asymmetric contacts is straightforward. In the next step, still for $U = 0$, we may also integrate over the dot degrees of freedom. We obtain the noninteracting generating function

$$Z_{ni}[\eta] = \prod_{\sigma} \det [-iG_{0\sigma}^{-1}(t, t') + \eta\Sigma^J(t, t')] , \quad (10)$$

where $G_{0\sigma}^{-1}(t, t')$ follows from

$$\begin{aligned} G_{0\sigma}(\omega) &= [(\omega - \epsilon_{0\sigma})\tau_z - \gamma_L(\omega) - \gamma_R(\omega)]^{-1} \\ &= \frac{1}{\Gamma^2 + (\omega - \epsilon_{0\sigma})^2} \\ &\times \begin{pmatrix} \omega - \epsilon_{0\sigma} + i\Gamma(F - 1) & i\Gamma F \\ i\Gamma(F - 2) & -\omega + \epsilon_{0\sigma} + i\Gamma(F - 1) \end{pmatrix} \end{aligned}$$

where τ_z is the standard Pauli matrix in Keldysh space, and $F = f(\omega + eV/2) + f(\omega - eV/2)$. Moreover, the self-energy for the source term is obtained as

$$\begin{aligned} \Sigma^J(t, t') &= \frac{e}{2} [\gamma_L(t, t') - \gamma_R(t, t')] \\ &\times [\delta(t - t_m) - \delta(t' - t_m)] . \end{aligned} \quad (11)$$

Up to this point, we have discussed the noninteracting case. In order to treat interactions, we now perform a Hubbard-Stratonovich transformation.

B. Hubbard-Stratonovich transformation

Let us therefore turn back to the real-time action S_{dot} of the dot in the presence of interactions, $U \neq 0$, see Eq. (6). For later numerical purpose, it is beneficial to proceed with the discussion in the time-discretized representation of the path integral [48]. In order to decouple the quartic term, we discretize the full time interval, $t = N\delta_t$, with the time increment δ_t . On each time slice, we perform a Trotter breakup of the dot propagator according to $e^{i\delta_t(H_0+H_T)} = e^{i\delta_t H_T/2} e^{i\delta_t H_0} e^{i\delta_t H_T/2} + O(\delta_t^2)$, where $H_0 = H_{dot} + H_{leads}$. By this, we introduce a Trotter error [49, 50, 51] which, however, will be eliminated from the results in a systematic way [52, 53], see below. Next, we use a discrete Hubbard-Stratonovich transformation [50, 54, 55] for the interacting part, which introduces Ising-like discrete spin fields $s_n^\pm = (s_n^+, s_n^-)$ on the $\alpha = \pm$ branches of the Keldysh contour (with $s_n^\alpha = \pm 1$) on the n -th Trotter slice. For a given Trotter slice, we now use

$$e^{\pm i\delta_t U (\hat{n}_\uparrow - \hat{n}_\downarrow)^2/2} = \frac{1}{2} \sum_{s^\pm = \pm} e^{-\delta_t \lambda_\pm s^\pm (\hat{n}_\uparrow - \hat{n}_\downarrow)} . \quad (12)$$

For $U > 0$, noting that $n_\uparrow - n_\downarrow = 0, \pm 1$, the sum can be carried out and gives the condition

$$\cosh(\delta_t \lambda_\pm) = \cos(\delta_t U/2) \pm i \sin(\delta_t U/2) .$$

The solution is $\lambda_\pm = \lambda' \pm i\lambda''$ with

$$\delta_t \lambda' = \sinh^{-1} \sqrt{\sin(\delta_t U/2)}, \quad \delta_t \lambda'' = \sin^{-1} \sqrt{\sin(\delta_t U/2)} . \quad (13)$$

Note that the overall sign of λ_\pm is chosen arbitrarily, but does not influence the physical result. Uniqueness of this Hubbard-Stratonovich transformation requires $U\delta_t < \pi$. To ensure sufficiently small time discretizations, in all calculations one should then obey the condition $\max(U, e|V|, |\epsilon_0|, T) \lesssim 1/\delta_t$.

C. Total GF and generating function

After the Hubbard-Stratonovich transformation, the remaining fermionic Grassmann variables $(\bar{d}_\sigma, d_\sigma)$ can be integrated out at the cost of the path summation over the HS Ising spins $\{s\}$,

$$Z[\eta] = \sum_{\{s\}} \prod_{\sigma} \det(-iG_{\sigma}^{-1}[\{s\}, \eta]) , \quad (14)$$

with the total Keldysh GF written in time-discretized ($1 \leq k, l \leq N$) form as

$$(G_{\sigma}^{-1})_{kl}^{\alpha\beta}[\{s\}, \eta] = (G_{0\sigma}^{-1})_{kl}^{\alpha\beta} + i\eta \Sigma_{kl}^{J, \alpha\beta} - i\delta_t \delta_{kl} \lambda_\alpha s_k^\alpha \delta_{\alpha\beta} , \quad (15)$$

where $\alpha, \beta = \pm$ labels the Keldysh branches, and the noninteracting GF is

$$G_{0\sigma, kl} = \int_{-\infty}^{\infty} \frac{d\omega}{2\pi} e^{i\delta_t(k-l)\omega} G_{0\sigma}(\omega) . \quad (16)$$

Note that $G_{0\sigma}(t, t')$ depends only on time differences due to time-translational invariance of the noninteracting part. Moreover, the self-energy kernel stemming from the external source term follows as

$$\Sigma_{kl}^{J, \alpha\beta} = \frac{e}{2} [\gamma_{L, kl}^{\alpha\beta} - \gamma_{R, kl}^{\alpha\beta}] [\delta_{mk} \delta_{\alpha,+} - \delta_{ml} \delta_{\beta,+}] , \quad (17)$$

where $\gamma_{p, kl} = \gamma_p(t_k - t_l)$ and the measurement time is $t_m = m\delta_t$.

IV. THE ITERATIVE PATH-INTEGRAL SCHEME

Let us now exploit the property (see, e.g., Ref. [56]) that each Keldysh component of $G_{0\sigma, kl}$ decays exponentially at long time differences ($|k - l| \rightarrow \infty$) for finite T , see Eq. (16). We denote the corresponding time scale (correlation or memory time) by τ_c . In Fig. 2 we show typical examples of $\text{Re } G_{0\uparrow, kl}^-$ for different bias voltages V . The exponential decrease with time is illustrated in the inset of Fig. 2(a) where the absolute value $|\text{Re } G_{0\uparrow, kl}^-|$ is again plotted for the same parameters, but in a log-linear representation. For large bias voltages and low enough temperatures, e.g., at $V \gtrsim \Gamma$

and $T \leq 0.2\Gamma$, the decay is superposed by an oscillatory behavior, see Fig. 2. Since the lead-induced correlation function decays as $\sim \cos[eV(t-t')/2]/\sinh[\pi T(t-t')]$, the respective correlations decay on a time scale given by $\tau_c^{-1} \sim \max(k_B T, eV)$. (The correlation function also has an additional ϵ_0 -dependence of the decay characteristics.) Thus, the exponential decay suggests to neglect lead-induced correlations beyond the correlation time τ_c . This motivates an iterative scheme which exactly takes into account the correlations within τ_c , but neglects them outside. The exponential decay has to be contrasted to the case $T = V = 0$, where correlations die out only algebraically, and our approach is not applicable.

Let us then face the remaining path sum in Eq. (14). In the discrete time representation, we denote with $t_0 = 0 < t_N = N\delta_t$ the initial and final time, and $t_k = k\delta_t$, see Fig. 1. The discretized GF and self-energy kernels for given spin σ are then represented as matrices of dimension $2N \times 2N$. For explicit calculations, we arrange the matrix elements related to Keldysh space (characterized by the Pauli matrices τ) and to physical times (t_k, t_l) as $\tau \otimes (k, l)$. In particular, the ordering of the matrix elements from left to right (and from top to bottom) represent increasing times. The lead-induced correlations thus decrease exponentially with growing distance from the diagonal of the matrix. For numerical convenience, we evaluate the generating function in the equivalent form

$$Z[\eta] = \mathcal{N} \sum_{\{s\}} \prod_{\sigma} \det D_{\sigma}[\{s\}, \eta], \quad (18)$$

with $D_{\sigma} = G_{0\sigma} G_{\sigma}^{-1}$. Explicitly, this reads

$$D_{\sigma, kl}^{\alpha\beta}[\{s\}, \eta] = \delta_{\alpha\beta} - i\delta_t \lambda_{\alpha} G_{0\sigma, kl}^{\alpha\beta} s_k^{\alpha} + i\eta \sum_{j, \alpha'} G_{0\sigma, kj}^{\alpha\alpha'} \Sigma_{jl}^{J, \alpha'\beta} \quad (19)$$

The normalization prefactor \mathcal{N} does not affect physical observables, and is put to unity. The time local nature of the on-dot interaction is now present only in disguise,

since the matrix product lets Ising spins appear line-wise. By construction, we have to sum over $2N$ auxiliary Ising spins, and the total number of possible spin configurations is 2^{2N} .

Next, we exploit the above-mentioned truncation of the GF by setting $D_{kl} \equiv 0$ for $|k-l|\delta_t > \tau_c$, where

$$\tau_c \equiv K\delta_t \quad (20)$$

is the memory time, with K the respective number of Trotter time slices. The GF matrices then have a K -band structure. Note that in the continuum limit, where $K = N, \delta_t \rightarrow 0$ and $N \rightarrow \infty$, the approach is exact.

To prepare the basis for the iterative scheme, we now transform the GF matrix to Schur's form, which then allows to calculate the determinant in a straightforward way. In general, a quadratic block matrix D given as $D = \begin{pmatrix} a & b \\ c & d \end{pmatrix}$, with a being invertible, can be represented in its Schur form, i.e., after one step of Gaussian elimination. Hence, by multiplying from the left with a lower triangular matrix,

$$\tilde{D} = LD = \begin{pmatrix} I_n & 0 \\ -ca^{-1} & I_m \end{pmatrix} \begin{pmatrix} a & b \\ c & d \end{pmatrix} = \begin{pmatrix} a & b \\ 0 & d - ca^{-1}b \end{pmatrix},$$

where $I_{n(m)}$ represent unit matrices of dimension $n = \dim a$ ($m = \dim d$), and b, c do not have to be quadratic themselves. Clearly, the determinant is invariant under this transformation. The $(2, 2)$ element in this block notation is often referred to as the Schur complement of the matrix D . This representation thus allows to write the determinant as $\det(D) = \det(a) \det(d - ca^{-1}b)$. We can now establish the iterative scheme as follows. We start from the full GF in the matrix representation as defined in Eq. (19). After the memory truncation, the $N \times N$ -matrix (in time space) assumes a band structure represented as

$$D \equiv D_{(1, N_K)} = \begin{pmatrix} \boxed{D^{11}} & \boxed{D^{12}} & 0 & 0 & \dots & 0 \\ \boxed{D^{21}} & \boxed{D^{22}} & \boxed{D^{23}} & 0 & \dots & \vdots \\ 0 & \boxed{D^{32}} & \boxed{D^{33}} & \boxed{D^{34}} & \dots & \vdots \\ 0 & 0 & \boxed{D^{43}} & \boxed{D^{44}} & \dots & 0 \\ \vdots & \vdots & \vdots & \vdots & \ddots & \boxed{D^{N_K-1, N_K}} \\ 0 & \dots & \dots & 0 & \boxed{D^{N_K, N_K-1}} & \boxed{D^{N_K, N_K}} \end{pmatrix}$$

where the single blocks are $K \times K$ -block matrices defined as ($l, l' = 1, \dots, N_K$)

$$\boxed{D^{ll'}} = \begin{pmatrix} D_{(l-1)K+1, (l'-1)K+1} & \dots & D_{(l-1)K+1, l'K} \\ \vdots & \ddots & \vdots \\ D_{lK, (l'-1)K+1} & \dots & D_{lK, l'K} \end{pmatrix}.$$

The number N of Trotter slices is always chosen such that $N_K \equiv N/K$ is integer. The elements D_{kl} are given in Eq. (19), with their dependence on the Ising spins s_k^\pm kept implicit. Each D_{kl} still has a 2×2 -Keldysh structure, and a 2×2 spin structure. Then, we rewrite the generating function (18) as

$$Z[\eta] = \sum_{s_1^\pm, \dots, s_N^\pm} \det \{ D^{11}[s_1^\pm, \dots, s_K^\pm] \} \\ \times \det \left\{ D_{(2, N_K)}[s_{K+1}^\pm, \dots, s_N^\pm] - D^{21}[s_{K+1}^\pm, \dots, s_{2K}^\pm] [D^{11}[s_1^\pm, \dots, s_K^\pm]]^{-1} D^{12}[s_{K+1}^\pm, \dots, s_{2K}^\pm] \right\}, \quad (21)$$

where the $N_K - 1 \times N_K - 1$ -matrix $D_{(2, N_K)}$ is obtained from $D_{(1, N_K)}$ by removing the first line and the first column.

In order to set up an iterative scheme, we use the following observation: to be consistent with the truncation of the correlations after a memory time $K\delta_t$, we have to neglect terms that directly couple Ising spins at time differences larger than the memory time. This is achieved by setting

$$D^{l+2, l+1} D^{l+1, l} [D^{l, l}]^{-1} D^{l, l+1} D^{l+1, l+2} \rightarrow 0 \quad (22)$$

within the Schur complement in each further iteration step. Note that we do not neglect the full Schur complement but only those parts which are generated in the second-next iteration step. With this, we rewrite the generating function as

$$Z[\eta] = \sum_{s_1^\pm, \dots, s_N^\pm} \det \{ D^{11}[s_1^\pm, \dots, s_K^\pm] \} \prod_{l=1}^{N_K-1} \det \left\{ D^{l+1, l+1}[s_{lK+1}^\pm, \dots, s_{(l+1)K}^\pm] \right. \\ \left. - D^{l+1, l}[s_{lK+1}^\pm, \dots, s_{(l+1)K}^\pm] [D^{l, l}[s_{(l-1)K+1}^\pm, \dots, s_{lK}^\pm]]^{-1} D^{l, l+1}[s_{lK+1}^\pm, \dots, s_{(l+1)K}^\pm] \right\}. \quad (23)$$

Then, one can exchange the sum and the product, and by reordering the sum over all Ising spins, one obtains

$$Z[\eta] = \sum_{s_{N-K+1}^\pm, \dots, s_N^\pm} Z_{N_K}[s_{N-K+1}^\pm, \dots, s_N^\pm], \quad (24)$$

where Z_{N_K} is the last element obtained from the iterative procedure defined by ($l = 1, \dots, N_K - 1$)

$$Z_{l+1}[s_{lK+1}^\pm, \dots, s_{(l+1)K}^\pm] = \sum_{s_{(l-1)K+1}^\pm, \dots, s_{lK}^\pm} \Lambda_l[s_{(l-1)K+1}^\pm, \dots, s_{lK}^\pm, s_{lK+1}^\pm, \dots, s_{(l+1)K}^\pm] Z_l[s_{(l-1)K+1}^\pm, \dots, s_{lK}^\pm]. \quad (25)$$

The *propagating tensor* Λ_l can be read off from Eq. (23) as

$$\Lambda_l = \det \left\{ D^{l+1, l+1}[s_{lK+1}^\pm, \dots, s_{(l+1)K}^\pm] \right. \\ \left. - D^{l+1, l}[s_{lK+1}^\pm, \dots, s_{(l+1)K}^\pm] [D^{l, l}[s_{(l-1)K+1}^\pm, \dots, s_{lK}^\pm]]^{-1} D^{l, l+1}[s_{lK+1}^\pm, \dots, s_{(l+1)K}^\pm] \right\}. \quad (26)$$

Note that we use here the notion of *tensor* in the sense of a multi-dimensional array and not in the strict mathematical sense defined by the transformation properties of this object, see also Ref. [57]. The iteration starts with $Z_1[s_1^\pm, \dots, s_K^\pm] = \det \{ D^{11}[s_1^\pm, \dots, s_K^\pm] \}$.

The current is numerically obtained by evaluating Eq. (5) for a small but fixed value of η ; we have taken $\eta =$

0.001 for all results shown below. By this, we obtain the full time-dependent current $I(t_m)$ as a function of the measurement time t_m ($0 \leq t_m \leq N\delta_t$). At short times, this shows a transient oscillatory or relaxation behavior, which then reaches a plateau value from which we read off the steady-state current I .

V. CONVERGENCE AND EXTRAPOLATION PROCEDURE

In order to render the scheme exact, we have to eliminate the two systematic errors which are still present up to this point, namely, (i) the Trotter error due to finite time discretization $\delta_t = t/N$, and (ii) the memory error due to a finite memory time $\tau_c = K\delta_t$. The scheme becomes exact by construction in the limit $K \rightarrow \infty$ and $\delta_t \rightarrow 0$. To perform this limit in a straightforward way is not possible due to the exponential dependence of the array sizes on K . However, unless temperature is very low, we can eliminate both errors from the numerical data in the following systematic way: (i) We choose a fixed time discretization δ_t and a memory time τ_c . A reasonable estimate for τ_c is the minimum of $1/|eV|$ and $1/T$ (see above). With that, we calculate the current $I(\delta_t, \tau_c)$, and, if desired, the differential conductance $dI(\delta_t, \tau_c)/dV$ (the derivative is performed numerically for a small $\Delta V = 0.01\Gamma$). The calculation is then repeated for different choices of δ_t and τ_c . (ii) Next, the Trotter error can be eliminated by exploiting the fact that it vanishes quadratically for $\delta_t \rightarrow 0$ [49, 50, 51]. For a fixed memory time τ_c , we can thus extrapolate and obtain $dI(\tau_c)/dV = dI(\delta_t \rightarrow 0, \tau_c)/dV$, which still depends on the finite memory time τ_c . The quadratic dependence on δ_t is illustrated in Fig. 3 for different values of U . Note that each line corresponds to the same fixed memory time $\tau_c = 0.5/\Gamma$. (iii) In a last step, we eliminate the memory error by extrapolating for $1/\tau_c \rightarrow 0$, and obtain the final numerically exact value $dI/dV = dI(\tau_c \rightarrow \infty)/dV$. For the dependence on $1/\tau_c$, we empirically find a regular and systematic behavior as shown in Fig. 4. The $\tau_c \rightarrow \infty$ value is approached with corrections of the order of $1/\tau_c$, see Fig. 4. However, it should be stressed that temperature and voltage affect the convergence properties in different ways, as is already clear from Fig. 2. Importantly enough, when T and V are such that the extrapolation scheme described above converges, numerical exactness is warranted.

We have implemented the iterative scheme together with the convergence procedure on standard Xeon 2GHz machines. Computations are then only possible for $K \leq 7$ due to the limited memory (RAM) resources available. Typical running times for the shown simulation data are approximately 15 hours for $K = 5$. With a second, parallelized version of the code, we have been able to take into account up to 2^{14} summands in Eq. (25), corresponding to $K = 7$, within passable running times of a few days.

VI. RESULTS

Next, we discuss the results obtained by the application of the iterative procedure to the Anderson model. As pointed out before, see Sec. III A, we consider the symmetric case, $\Gamma_R = \Gamma_L = \Gamma/2$, with $\mu_{L/R} = \pm eV/2$. In what follows, we measure energies in units of Γ . Un-

less noted otherwise, all error bars for the shown data points, which are due to the Trotter and memory extrapolation scheme, are of the order of the symbol sizes in the figures. Our scheme yields the full time-dependent current $I(t)$, including transients as well as the asymptotic steady-state value. Fig. 5 shows typical results for the current $I(t)$, for two parameter sets, namely (1) $U = 4\Gamma, eV = 2\Gamma, T = 0.1\Gamma$ (black circles), and (2) $U = 0.5\Gamma, eV = 0.6\Gamma, T = \Gamma$ (red squares). The first set is of interest in the context of the nonequilibrium Kondo effect, where the Kondo temperature (for $\epsilon_0 = 0$) is $T_K = \sqrt{\Gamma U/2} \exp(-\pi U/8\Gamma)$; for parameter set (1), this yields $T_K = 0.29\Gamma$. For $eV \gg T_K$, analytical results for the steady-state current are available [12, 58], shown as solid line in Fig. 5. This indicates that the ISPI method is capable of approaching the nonequilibrium Kondo problem. For both parameter sets, and for many others not shown here, we observe that after a transient relaxation behavior, $I(t)$ settles at a plateau value, which then defines the stationary current discussed in the following.

A. Validation of the algorithm: comparison with exact and perturbative results

As a simple warm-up check, let us briefly compare our numerical results to the exact result for $U = 0$. Figure 6(a) shows the stationary current (obtained already at $t_m = 10/\Gamma$) as a function of ϵ_0 for $T = 0.1\Gamma$ and $eV = 0.2\Gamma$. The I - V characteristics is shown in Fig. 6(b) for $T = 0.1\Gamma$ and $\epsilon_0 = 0$. Both cases illustrate that the numerical result coincides with the exact one. Other parameter sets have been checked as well, and agree with the well-known $U = 0$ analytical solution.

Second, in order to validate the reliability of our code for finite U , we compare the numerical results to a perturbative calculation, where the interaction self-energy is computed up to second order in U [59]. In order to respect current conservation, this calculation is possible only at the electron-hole symmetric point, $\epsilon_0 = B = 0$ [18]. First-order terms give then no contribution, and the self-energy corresponds to just one diagram [59]. For a detailed comparison, we plot mostly the *interaction corrections*, $\delta A \equiv A(U) - A(U = 0)$, with A being the current I , the linear conductance G , or the nonlinear conductance dI/dV , respectively. Figure 7 shows the results for δI as a function of the bias voltage for $U = 0.1\Gamma$ and $U = 0.3\Gamma$. For $U = 0.1\Gamma$, we perfectly recover the perturbative results, which confirms the reliability of our code even in the regime of nonlinear transport. Clearly, the corrections are small and negative, which can be rationalized in terms of Coulomb blockade physics, as transport is suppressed by a finite interaction on the dot.

For $U = 0.3\Gamma$, the current decreases even more, and the deviations between the ISPI and perturbative results are also larger. The relative deviation for $U = 0.3\Gamma$ is already $\approx 30 - 35\%$, illustrating that perturbation theory

is already of limited accuracy in this regime. Although it well reproduces the overall tendency, there is significant quantitative disagreement. The differences are even more pronounced for $U = \Gamma$, as shown in Fig. 8 for δI (main) and for $\delta(dI/dV)$ (inset). Here, second-order perturbation theory does not even reproduce qualitative features.

B. Comparison with master equation approach

Next, we compare our numerical approach with the outcome of a standard master equation calculation [41]. The master equation is expected to yield reliable results in the incoherent (sequential) tunneling regime, $T \gg \Gamma$, where a description in terms of occupation probabilities for the isolated many-body dot states is appropriate. The transport dynamics is then described by a rate equation for the populations, where the time-dependent rates are obtained from lowest-order perturbation theory in Γ [41]. The results are shown for $U = \Gamma$ in Fig. 9, both for the nonlinear and the linear differential conductance interaction corrections. As temperature is lowered, interaction effects become more important, as seen from the exact ISPI results. This corresponds to the emergence of coherence effects for $T < \Gamma$, which are clearly not captured by the master equation in the sequential tunneling approximation. However, for $T \gtrsim 4\Gamma$, interaction corrections are washed out, and the master equation becomes essentially exact, cf. Fig. 9. Similarly, from our ISPI results, we observe that interaction corrections are suppressed by an increasing bias voltage as well. To give numbers, for $T = 1.25\Gamma$, we find in the linear regime $\delta G = -0.073e^2/h$, whereas $\delta(dI/dV) = -0.062e^2/h$ for $eV = 3\Gamma$.

C. Small bias: $eV \ll \Gamma$

For sufficiently small bias voltage, the current is linear in V , and we can focus on the linear conductance and its interaction correction δG . Figure 10 shows δG as a function of ϵ_0 for different magnetic fields B , taking $U = \Gamma$ and $T = 0.1$ (to be specific, we have chosen $eV = 0.05\Gamma$). For $B = 0$, two spin-degenerate transport channels contribute, and a single resonant-tunneling peak at $\epsilon_0 = 0$ results. The interaction corrections are most pronounced on resonance, $\epsilon_0 = 0$. For $B \neq 0$, the spin-dependent channels are split by $\Delta\epsilon = 2B$, resulting in a double-peak structure. The spin-resolved levels are now positioned at $\epsilon_0 \pm B$ due to the Zeeman splitting. Again the interaction corrections are largest on resonance, and the double-peak structure of $G(\epsilon_0)$ is transferred to $\delta G(\epsilon_0)$, cf. Fig. 10. We find no evidence for an interaction-induced broadening of the resonant-tunneling peak compared to the noninteracting case. The width of the Lorentzian peak profile for $B = 0$ is determined by Γ at sufficiently low T , and broadens as T increases. Here, the double-peak structure, with two clearly separated peaks for finite B , is not

yet fully developed. The two peaks largely overlap, and the distance of the peaks is below the expected $\Delta\epsilon = 2B$, since tunneling considerably broadens the dot levels. We note however, that for larger B , the correct peak spacing of $\Delta\epsilon = 2B$ is reproduced (data not shown).

In order to illustrate the role of the interaction U , we show the dependence of δG on U at $\epsilon_0 = 0$ in the inset of Fig. 10. For $U = 0$, both levels contribute e^2/h to the conductance at low temperatures, while for finite U these contributions are reduced. The reduction increases with growing U , qualitatively consistent with previous results. The interaction corrections are smaller away from resonance, see inset of Fig. 10, but they also grow with increasing U .

Next, we address the temperature dependence of the linear conductance (numerically evaluated for $eV = 0.05\Gamma$). In Fig. 11, we show $G(T)$ for different values of U (up to $U = 4\Gamma$) at $\epsilon = B = 0$. For $U = 1.2\Gamma$, the deviation from the $U = 0$ -result is small in the considered temperature range. For larger U , deviations become more pronounced at low temperatures where interaction becomes increasingly relevant. Up to present, we have obtained converged results in the regime of *small* bias voltages for interaction strengths $U \leq 4\Gamma$ for temperatures above or close to the Kondo temperature, $T \gtrsim T_K$. The corresponding Kondo temperatures are (see above) $T_K = 0.38\Gamma$ for $U = 3\Gamma$ and $T_K = 0.293\Gamma$ for $U = 4\Gamma$. In the regime $T_K \lesssim T \lesssim 10T_K$, we can compare our results to the result of Hamann [60, 61],

$$G(T) = \frac{e^2}{h} \left(1 - \frac{\ln(T/T_{KH})}{[\ln^2(T/T_{KH}) + 3\pi^2/4]^{1/2}} \right), \quad (27)$$

for the linear conductance, where $T_{KH} = T_K/1.2$, see Fig. 11 (solid lines). In Ref. [60], it has been shown that the results of the numerical RG coincide with those of Eq. (27) in this regime. Fig. 11 illustrates that the agreement between the two approaches is satisfactory and shows that the ISPI provides reliable results in the linear regime above or close to the Kondo temperature. As already mentioned, convergence is problematic in the *linear* regime for temperatures lower than the Kondo temperature for larger values of U . This implies that the equilibrium Kondo regime is difficult to explore using the ISPI approach. However, the situation is more favorable for large bias voltages, where short to intermediate memory times are sufficient, and we have achieved convergence up to $U = 4\Gamma$, see Fig. 5 and the next subsection.

D. Large bias: $eV \geq \Gamma$

Let us then turn to nonequilibrium transport at voltages $eV \gtrsim \Gamma$. Here, the transport window is $\sim eV$, and a double-peak structure for dI/dV emerges even for $B = 0$, with distance eV between the peaks. As interaction corrections to the nonlinear conductance are largest when a dot level is in resonance with one of the chemical potentials of the leads, the double-peak structure is again

transferred to $\delta(dI/dV)$. This can be observed in Fig. 12, where we show results for $eV = 3\Gamma$ but otherwise the same parameters as in Fig. 10. For a finite magnetic field, each peak of the double-peak structure itself experiences an additional Zeeman splitting, resulting in an overall four-peak structure. For $B = \Gamma$ and the shown values of U , the two innermost peaks (closest to $\epsilon_0 = 0$) overlap so strongly that they effectively form a single peak at $\epsilon_0 = 0$ again. The two outermost peaks are due to the combination of the finite magnetic field and the bias voltage.

Increasing the on-dot interaction U leads to a reduction of the differential conductance peaks compared to the noninteracting case, i.e., the interaction corrections are again largest when the level energy matches the chemical potential in the leads. This is observed in the inset of Fig. 12, for $B = 0$ and $\epsilon_0 = -\Gamma$, which is close to the peak maximum. Away from resonance, the interaction corrections are reduced. Note that the four-peak structure is already present in the noninteracting case (with $B \neq 0$) and, hence, is not modified qualitatively by U .

In the regime $eV \gg T_K$, we can compare our results to the perturbative RG result [12, 58]

$$I(V) = \frac{3\pi^2 e^2 V}{8h} \ln^{-2}(eV/\tilde{T}_K),$$

with $\tilde{T}_K = 2T_K/\sqrt{\pi}$. Fig. 5 shows the result for the stationary current for $U = 4\Gamma$ (where $T_K = 0.29\Gamma$) for $eV = 2\Gamma$. The perturbative current amounts to $I_\infty = 2.28e\Gamma/h$, while the ISPI value is $I_{ISPI} = 2.25e\Gamma/h$. The quite satisfactory agreement suggests that ISPI is indeed a reliable new method that holds promise for reaching the nonequilibrium Kondo regime. A detailed study of the nonequilibrium Kondo effect using ISPI will be given elsewhere.

Finally, we address the temperature dependence of the nonlinear conductance dI/dV . ISPI results for $eV = 2\Gamma, \epsilon_0 = B = 0$ are shown in Fig. 13. Again, as in the linear regime, the conductance increases with lower temperatures, and finally saturates, e.g., at $dI/dV = e^2/h$ for $U = 0$ and $eV = 2\Gamma$. Clearly the conductance decreases when the bias voltage is raised. Increasing U renders this suppression yet more pronounced, see also inset of Fig. 13 for the corresponding corrections. At high temperatures, thermal fluctuations wash out the interaction effects, and the interaction corrections die out.

VII. DISCUSSION AND CONCLUSIONS

In summary, we have introduced a scheme for the iterative summation of real-time path integrals (ISPI), and applied it to a prototypical problem of quantum transport through an interacting quantum dot coupled to metallic leads held at different chemical potentials. After integrating out the leads, a time-nonlocal Keldysh self-energy arises. Exploiting the exponential decay of

the time correlations at finite temperature allows to introduce a memory time τ_c beyond which the correlations can be truncated. Within τ_c , correlations are fully taken into account in the corresponding path integral for the current generating function. Then, through a discrete Hubbard-Stratonovich transformation, interactions can be transferred to an auxiliary spin field, and an iterative summation scheme has been constructed to calculate the transport current. The remaining systematic errors due to the finite time discretization and the finite memory time τ_c are then eliminated by a refined Hirsch-Fye-type extrapolation scheme, rendering the ISPI numerically exact. From this construction, it is clear that the calculation is reliable for temperatures above a certain interaction-dependent temperature scale. The latter depends also on the computational power available, and vanishes in the absence of interactions.

The general scheme has been applied to the canonical example of an Anderson dot with interaction U , for which many features of the transport characteristics are well understood. This allows to carefully and systematically check the algorithm. In the regime of linear transport, we have recovered results from second-order perturbation theory in U in the limit of very small interaction strength, but found significant deviations already for small-to-intermediate values of U . In the incoherent sequential regime, we recover results from a master equation approach. Taking $U/\Gamma = 4$, we have furthermore reproduced the behavior of the linear conductance above the Kondo temperature and found satisfactory agreement with numerical RG results. In addition, we have investigated the regime of correlated nonlinear transport, where, in our opinion, the presented method is most valuable. We have checked that for large voltage, known results on the nonequilibrium Kondo effect are reproduced as well.

Up to now, we have achieved converged results for small-to-intermediate U even at rather low temperatures and small bias voltages. However, the strong-coupling regime of the Kondo effect has not yet been fully captured, as the required memory times become quite large, and, at the same time, small δ_t are necessary because of the large U . This combined requirement makes it difficult to reach convergence. Nevertheless, the *nonequilibrium* Kondo regime, representing an intermediate-to-weak coupling situation, seems tractable by the ISPI scheme. The applicability and accuracy of ISPI has been demonstrated for bias voltages larger than the Kondo temperature. We will present a detailed study of this interesting regime elsewhere.

Our approach is, in fact, similar in spirit to the well-established concept of the quasi-adiabatic path integral (QUAPI) scheme, introduced by Makri and Makarov [57] in its iterative version. This method has been developed to describe the dynamics of a quantum system coupled to a bath of harmonic oscillators held at equilibrium, in order to obtain exact results for quantum decoherence and dissipation, see also Refs. [53, 62]. For a dipole-type

system-bath coupling, as it occurs, e.g., in the spin-boson model [56], the bath-induced correlations are encoded in the Feynman-Vernon influence functional [63], which is solely a functional of a single *system* operator, say \hat{x} , which couples the system to the bath. The very existence of this functional allows to perform a basis rotation to the eigenbasis of \hat{x} (called the discrete variable representation, DVR). Then, the influence functional can be evaluated at the eigenvalues of \hat{x} during the numerical calculation of the real-time path integral over $\hat{x}(t)$. Moreover, within the QUAPI scheme, the influence functional also generates correlations which are non-local in time, but which also decay exponentially. This allows to truncate them beyond a memory-time τ_{mem} , which coincides conceptually with our correlation time τ_c . Then, in practice, numerical convergence has to be achieved with respect to the memory time [53]. Afterwards, the only remaining Trotter error can be completely eliminated by extrapolation [53]. In the present case of nonequilibrium transport, several fundamental differences occur, and, in fact, only the strategy of memory truncation can be taken over. The major difference is that there exists no simple Feynman-Vernon influence functional. While the lead fermions can be integrated out, see Eq. (8), the corresponding Grassmann variables for the dot cannot be transferred to a practical computational scheme along the lines of the QUAPI method. Instead, here we integrate out *all* fermions, at the expense of introducing auxiliary Ising spins via the HS transformation. Then, ISPI performs a summation over these Ising spins. Another difference is the form of the tunnel coupling in the Hamiltonian. As two non-commuting system operators

d_σ and d_σ^\dagger occur, no analogue of DVR can be established here.

Finally, we note that we have chosen the Anderson model as a simple but non-trivial toy model for quantum transport in order to establish and test the numerical algorithm. We believe that this approach, or modifications thereof, will be of importance in numerical calculations of quantum transport properties. Compared to other approaches, it has several advantages (e.g., numerical exactness, direct nonequilibrium formulation, no sign problem), but is, on the other hand, also computationally more costly than most other techniques, especially for strong correlations and/or low energy scales (temperature, voltage). In any case, it goes without saying that other interesting models for quantum transport exist, and future work will be devoted to apply ISPI to those.

Acknowledgments

We acknowledge financial support within the DFG priority program 1243 “Quantum transport at the molecular scale” and by the SFB Transregio 12. We thank L. Dell’Anna for providing the results of the nonequilibrium perturbation theory, and for discussions. We also thank K. Flensberg, A.-P. Jauho and J. Paaske for useful discussions, and for the kind hospitality at the Niels-Bohr Institute of the University of Copenhagen (M.T.), where parts of this work have been completed. Computational time from the ZIM at the Heinrich-Heine-Universität Düsseldorf is acknowledged.

-
- [1] T. Heinzl, *Mesoscopic Electronics in Solid State Nanostructures*, 2nd ed. (VCH-Wiley, Berlin, 2006).
 - [2] *Introducing Molecular Electronics*, G. Cuniberti, G. Fagas, K. Richter (eds.), Lecture Notes in Physics, (Springer, Heidelberg, 2005).
 - [3] M. Galperin, M.A. Ratner, and A. Nitzan, J. Phys. Cond. Matt. **19**, 103201 (2007).
 - [4] J. Reichert, R. Ochs, D. Beckmann, H. B. Weber, M. Mayor, and H. v. Löhneysen, Phys. Rev. Lett. **88**, 176804 (2002).
 - [5] R. Smit, Y. Noat, C. Untiedt, N. D. Lang, M. C. van Hemert, and J. M. Ruitenbeek, Nature **419**, 906 (2002).
 - [6] T. Böhler, J. Grebing, A. Mayer-Gindner, H. v. Löhneysen, and E. Scheer, Nanotechnology **15**, 465 (2004).
 - [7] H. Park, J. Park, A.K.L. Kim, E.H. Anderson, A.P. Alivisatos, and P.L. McEuen, Nature **407**, 57 (2000).
 - [8] J. König, J. Schmid, H. Schoeller, and G. Schön, Phys. Rev. B **54**, 16820 (1996).
 - [9] Y. Meir and N.S. Wingreen, Phys. Rev. Lett. **68**, 2512 (1992).
 - [10] S. Hershfield, J.H. Davies, and J.W. Wilkins, Phys. Rev. B **46**, 7046 (1992).
 - [11] D.A. Abanin and L.S. Levitov, Phys. Rev. Lett. **94**, 186803 (2005).
 - [12] A. Kaminski, Yu.V. Nazarov, and L.I. Glazman, Phys. Rev. B **62**, 8154 (2000).
 - [13] A. Mitra, and A.J. Millis, Phys. Rev. B **76**, 085342 (2007).
 - [14] A. Oguri, Phys. Rev. B **64**, 153305 (2001).
 - [15] A.A. Aligia, Phys. Rev. B **74**, 155125 (2006).
 - [16] R.M. Konik, H. Saleur, and A. Ludwig, Phys. Rev. B **66**, 125304 (2002).
 - [17] A. Rosch, J. Paaske, J. Kroha, and P. Wölfle, Phys. Rev. Lett. **90**, 076804 (2003).
 - [18] T. Fujii and K. Ueda, Phys. Rev. B **68**, 155310 (2003); J. Phys. Soc. Jpn. **74**, 127 (2005).
 - [19] K.S. Thygesen and A. Rubio, Phys. Rev. B **77**, 115333 (2008).
 - [20] A. Komnik and A.O. Gogolin, Phys. Rev. Lett. **90**, 246403 (2003).
 - [21] B. Doyon and N. Andrei, Phys. Rev. B **73**, 245326 (2006).
 - [22] P. Mehta and N. Andrei, Phys. Rev. Lett. **96**, 216802 (2006).
 - [23] L. Borda, K. Vladar, and A. Zawadowski, Phys. Rev. B **75**, 125107 (2007).
 - [24] B. Doyon, Phys. Rev. Lett. **99**, 076806 (2007).
 - [25] E. Boulat and H. Saleur, Phys. Rev. B **77**, 033409 (2008).

- [26] A. Nishino and N. Hatano, J. Phys. Soc. Jap. **76**, 063002 (2007).
- [27] H. Schoeller and J. König, Phys. Rev. Lett. **84**, 3686 (2000).
- [28] D. Bohr and P. Schmitteckert, Phys. Rev. B **75**, 241103(R) (2007); P. Schmitteckert and F. Evers, Phys. Rev. Lett. **100**, 086401 (2008).
- [29] A.J. Daley, C. Kollath, U. Schollwöck, and G. Vidal, J. Stat. Mech.: Theor. Exp. P04005 (2004).
- [30] S.G. Jakobs, V. Meden, and H. Schoeller, Phys. Rev. Lett. **99**, 150603 (2007).
- [31] T.A. Costi, Phys. Rev. B **55**, 3003 (1997).
- [32] Very recent progress on the application of the numerical renormalization group method out of equilibrium has been reported by F.B. Anders and A. Schiller, Phys. Rev. B **74**, 245113 (2006); F.B. Anders, preprint arXiv:0802.0371.
- [33] A. Oguri, H. Ishii, and T. Saso, Phys. Rev. B **51**, 4715 (1995).
- [34] X. Wang, C.D. Spataru, M.S. Hybertsen, and A.J. Millis, Phys. Rev. B **77**, 045119 (2008).
- [35] C.H. Mak and R. Egger, J. Chem. Phys. **110**, 12 (1999); R. Egger, L. Mühlbacher, and C.H. Mak, Phys. Rev. E **61**, 5961 (2000).
- [36] L. Mühlbacher and R. Egger, J. Chem. Phys. **118**, 179 (2003).
- [37] L. Mühlbacher and E. Rabani, Phys. Rev. Lett. **100**, 176403 (2008).
- [38] S. Kehrein, Phys. Rev. Lett. **95**, 056602 (2005).
- [39] J.E. Han and R.J. Heary, Phys. Rev. Lett. **99**, 236808 (2007).
- [40] P.W. Anderson, Phys. Rev. **124**, 41 (1961).
- [41] H. Bruus and K. Flensberg, *Many-Body Quantum Theory in Condensed Matter Physics*, (Oxford UP, Oxford, 2004).
- [42] A. M. Tsvelik and P. B. Wiegmann, Adv. Phys. **32**, 453 (1983).
- [43] A. Schiller and S. Hershfield, Phys. Rev. B **51**, 12896 (1995).
- [44] B. Horváth, B. Lazarovits, O. Sauret, and G. Zaránd, Phys. Rev. B **77**, 113108 (2008).
- [45] A. Kamenev, in *Nanophysics: Coherence and Transport*, Les Houches session LXXXI, ed. H. Bouchiat, Y. Gefen, S. Guéron, G. Montambaux, and J. Dalibard (Elsevier, New York, 2005).
- [46] L.V. Keldysh, Zh. Eksp. Teor. Fiz., **47**, 1515 (1964) [Sov. Phys. JETP **47**, 804 (1961)].
- [47] J. Rammer and H. Smith, Rev. Mod. Phys. **58**, 323 (1986).
- [48] J.W. Negele and H. Orland, *Quantum Many-Particle Systems* (Addison-Wesley, Redwood City, 1988).
- [49] J.E. Hirsch, and R.M. Fye, Phys. Rev. Lett. **56**, 2521 (1986).
- [50] J.E. Hirsch, Phys. Rev. B **28**, 4059 (1983).
- [51] R.M. Fye, Phys. Rev. B **33**, 6271 (1986).
- [52] H. De Raedt, and B. De Raedt, Phys. Rev. A **28**, 3575 (1983).
- [53] J. Eckel, S. Weiss, and M. Thorwart, Eur. Phys. J. B **53**, 91 (2006).
- [54] J. Hubbard, Phys. Rev. Lett. **3**, 77 (1959).
- [55] F. Siano and R. Egger, Phys. Rev. Lett. **93**, 047002 (2004).
- [56] U. Weiss, *Quantum Dissipative Systems*, 2nd ed. (World Scientific, Singapore, 1999).
- [57] D.E. Makarov and N. Makri, Chem. Phys. Lett. **221**, 482 (1994); N. Makri and D.E. Makarov, J. Chem. Phys. **102**, 4600 (1995); N. Makri and D.E. Makarov, J. Chem. Phys. **102**, 4611 (1995); N. Makri, J. Math. Phys. **36**, 2430 (1995).
- [58] A. Rosch, J. Paaske, J. Kroha, and P. Wölfle, J. Phys. Soc. Jap. **74**, 118 (2005).
- [59] L. Dell'Anna, A. Zazunov, and R. Egger, Phys. Rev. B **77**, 104525 (2008).
- [60] T.A. Costi, A.C. Hewson, and V. Zlatic, J. Phys.: Condens. Matter **6**, 2519 (1994).
- [61] D.R. Hamann, Phys. Rev. **158**, 570 (1967).
- [62] M. Thorwart and P. Jung, Phys. Rev. Lett. **78**, 2503 (1997); M. Thorwart, P. Reimann, P. Jung, and R.F. Fox, Chem. Phys. **235**, 61 (1998); M. Thorwart, P. Reimann, P. Jung and R.F. Fox, Phys. Lett. A **239**, 233 (1998); M. Thorwart, P. Reimann, and P. Hänggi, Phys. Rev. E **62**, 5808 (2000); M. Thorwart, E. Paladino, and M. Grifoni, Chem. Phys. **296**, 333 (2004); M.C. Goorden, M. Thorwart, and M. Grifoni, Phys. Rev. Lett. **93**, 267005 (2004); M. Thorwart, J. Eckel and E.R. Mucciolo, Phys. Rev. B **72**, 235320 (2005).
- [63] R. Feynman and F.L. Vernon, Ann. Phys. (N.Y.) **24**, 118 (1963).

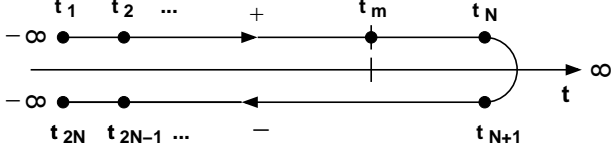


FIG. 1: Keldysh contour: every physical time has two contour representatives on the branches \pm . The measurement time t_m only has a single representative on the upper branch.

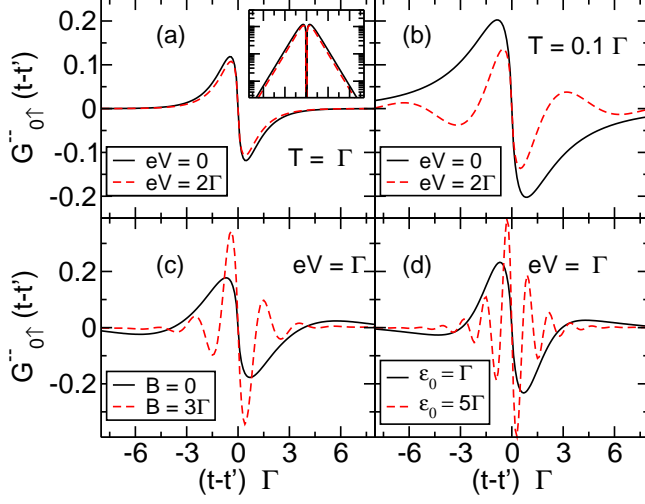


FIG. 2: (Color online) Real part of the Keldysh GF component $G_{0\uparrow}^{--}(t-t')$ for (a) $\epsilon_0 = 0, B = 0, T = \Gamma$, (b) $\epsilon_0 = 0, B = 0, T = 0.1\Gamma$, (c) $\epsilon_0 = 0, T = 0.1\Gamma, eV = \Gamma, B = 0$ and $B = 3\Gamma$, (d) $B = 0, T = 0.1\Gamma, eV = \Gamma, \epsilon_0 = \Gamma$ and $\epsilon_0 = 5\Gamma$. The inset in (a) shows the absolute values of the same data in log-linear representation, highlighting the exponential decrease.

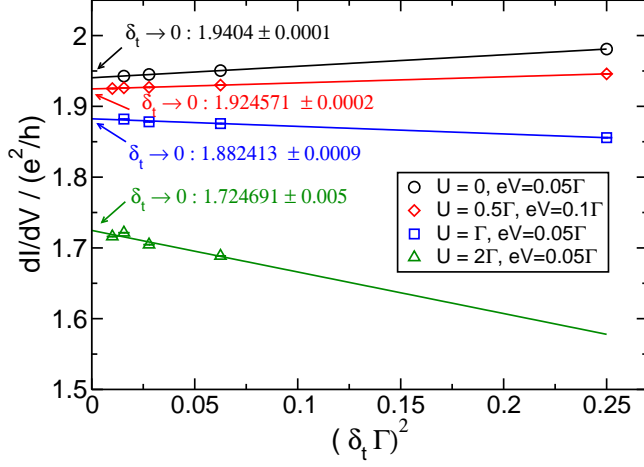


FIG. 3: (Color online) Quadratic dependence of the Trotter error as obtained in the convergence procedure for $\delta t \rightarrow 0$ for a fixed memory time $\tau_c = 0.5/\Gamma$. Parameters are $\epsilon_0 = 0, B = 0, T = 0.1\Gamma$. The extrapolated values are given in the figure.

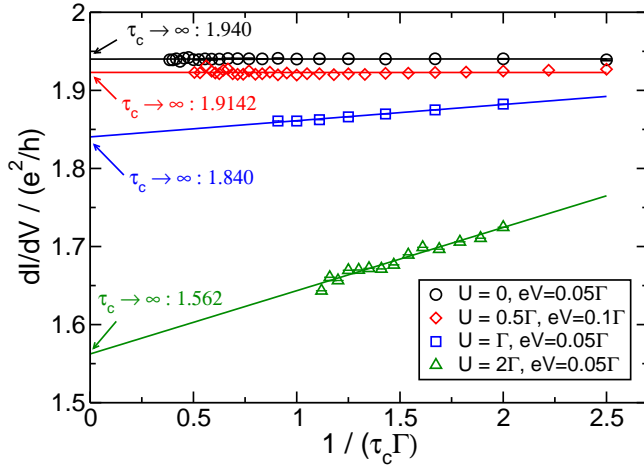


FIG. 4: (Color online) Dependence of the differential conductance $dI(\tau_c)/dV$ on the inverse memory time $1/\tau_c$ for different values of U after the Trotter error has been eliminated. Parameters are $\epsilon_0 = B = 0, T = 0.1\Gamma$. Solid lines correspond to a linear fit. The extrapolated values for $dI/dV = dI(1/\tau_c \rightarrow 0)/dV$ are given in the figure.

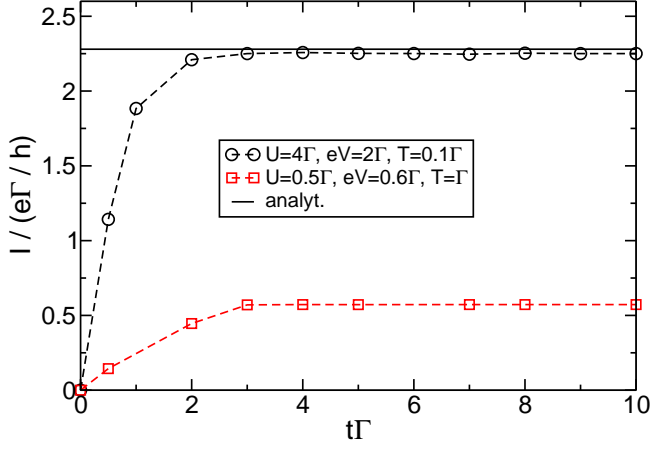


FIG. 5: (Color online) Time-dependent current $I(t)$ for two representative parameter sets: (1) $U = 4\Gamma, eV = 2\Gamma, T = 0.1\Gamma$ (black circles) and (2) $U = 0.5\Gamma, eV = 0.6\Gamma, T = \Gamma$ (red squares). Solid line: analytical result for stationary I from nonequilibrium Kondo theory applied to parameter set (1) [12, 58]. Symbols are ISPI results, dashed lines are guides to the eye only, and $\epsilon_0 = B = 0$.

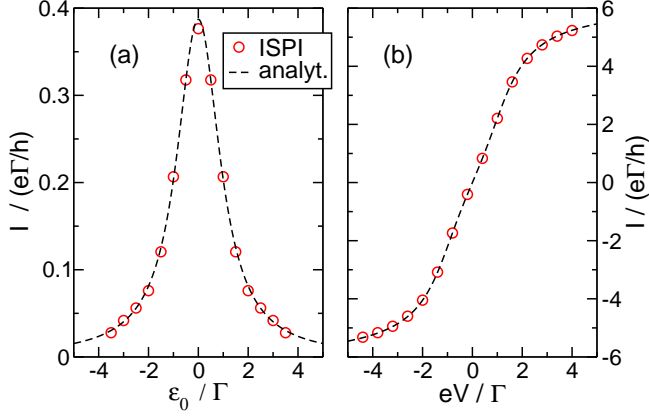


FIG. 6: (Color online) Stationary current as a function of ϵ_0 (a) and of the bias voltage eV (b) for the noninteracting case $U = 0$. Shown are the numerical (circles) and the exact analytical (dashed curve) results for (a) $eV = 0.2\Gamma$, and (b) $\epsilon_0 = 0$. In both cases, $T = 0.1\Gamma, B = 0$.

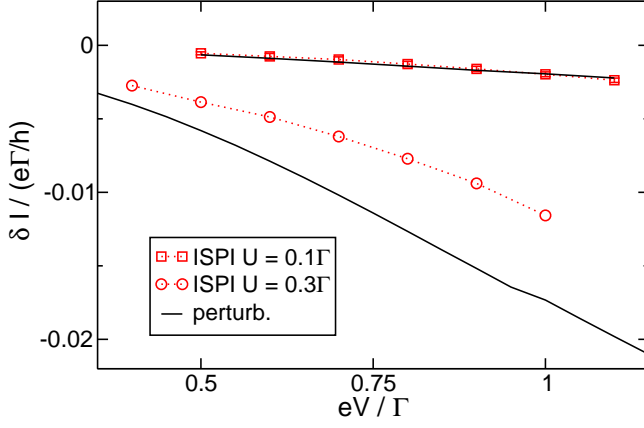


FIG. 7: (Color online) Interaction corrections $\delta I(V) = I(U) - I(U = 0)$ from the numerical ISPI approach (red symbols) and from a second-order perturbative calculation (black solid lines), for $U = 0.1\Gamma$ (squares) and $U = 0.3\Gamma$ (circles). Parameters are $\epsilon_0 = B = 0, T = 0.1\Gamma$, and dotted lines are guides to the eye only.

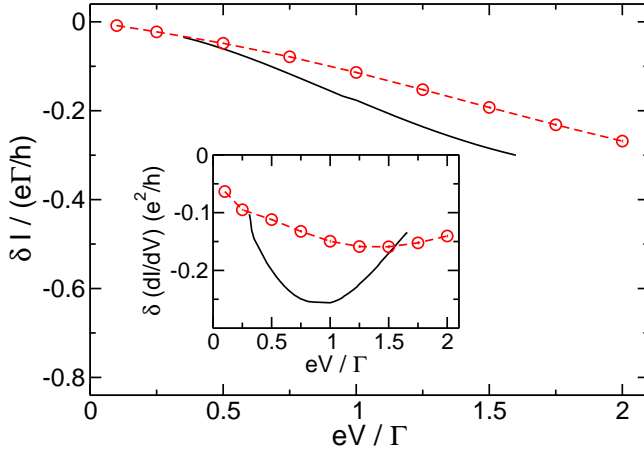


FIG. 8: (Color online) Interaction correction δI for the non-linear current for $U = \Gamma$, comparing ISPI (red symbols) and U^2 perturbation theory (black solid curve). The inset shows the corresponding interaction corrections $\delta(dI/dV)$ to the differential conductance. Other parameters are as in Fig. 7. Dashed lines are guides to the eye only.

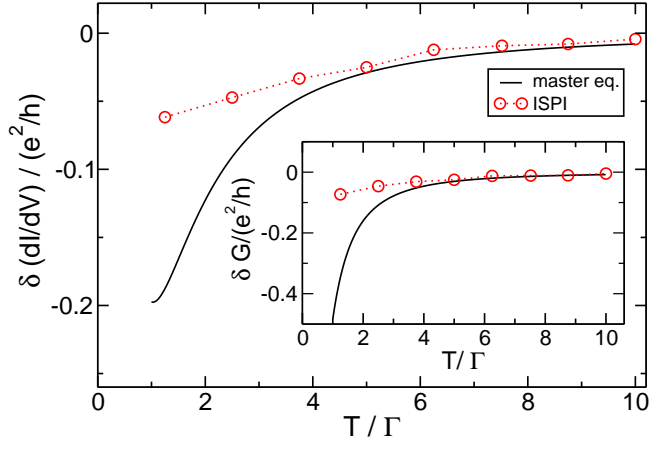


FIG. 9: (Color online) Comparison of the ISPI method (red symbols) and the master equation approach (solid lines) for $U = \Gamma$. Main: Corrections $\delta(dI/dV)$ of the nonlinear conductance as a function of temperature for $eV = 3\Gamma$. Inset: Same for the linear conductance δG . For the remaining parameters, see Fig. 7.

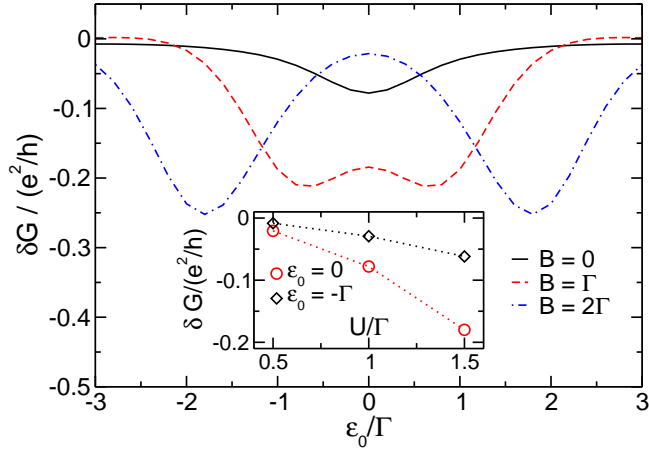


FIG. 10: (Color online) Interaction correction δG as a function of ϵ_0 , for $U = \Gamma$, different B , and $T = 0.1\Gamma$. Inset: Dependence of δG on U for $B = 0$, on resonance ($\epsilon_0 = 0$, red circles) and away from resonance ($\epsilon_0 = -\Gamma$, black diamonds).

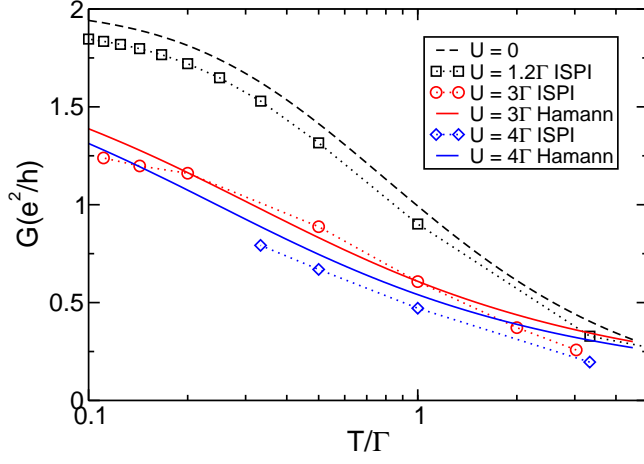


FIG. 11: (Color online) Linear conductance G vs temperature T , for $U = 0$ (dashed line) and $U = 1.2, 3, 4\Gamma$ ($\epsilon_0 = B = 0$). Symbols denote the ISPI results while the solid lines are those of Eq. (27).

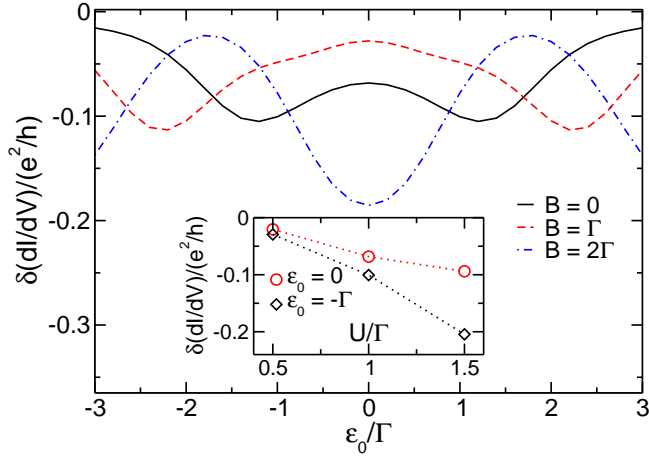


FIG. 12: (Color online) Same as Fig. 10 but for the nonlinear conductance, taken at $eV = 3\Gamma$.

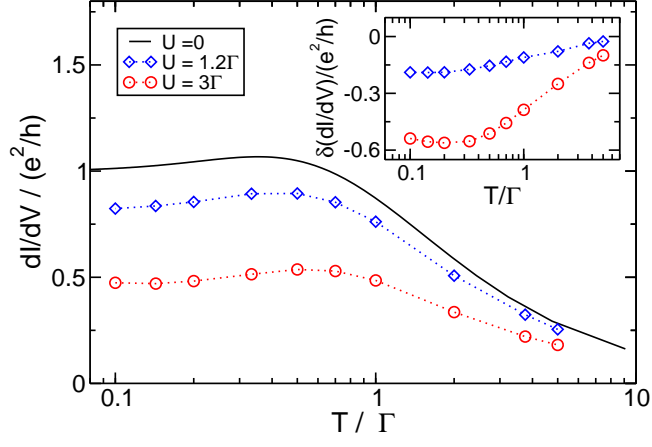


FIG. 13: (Color online) Nonlinear differential conductance dI/dV vs temperature T , for $eV = 2\Gamma$, $\epsilon_0 = B = 0$, and $U = 0, 1.2, 3\Gamma$. Inset: corresponding interaction corrections $\delta(dI/dV)$. (The Kondo temperature for $U = 3\Gamma$ is $T_K = 0.38\Gamma$.)